Enhanced Photosynthesis and Growth in *atquac1* Knockout Mutants Are Due to Altered Organic Acid Accumulation and an Increase in Both Stomatal and Mesophyll Conductance[1]

David B. Medeiros, Samuel C.V. Martins, João Henrique F. Cavalcanti, Danilo M. Daloso, Enrico Martinoia, Adriano Nunes-Nesi, Fábio M. DaMatta, Alisdair R. Fernie, and Wagner L. Araújo*

Departamento de Biologia Vegetal (D.B.M., S.C.V.M, J.H.F.C., A.N.-N., F.M.D., W.L.A.) and Max-Planck Partner Group at the Departamento de Biologia Vegetal (D.B.M., J.H.F.C., A.N.-N., W.L.A.), Universidade Federal de Viçosa, 36570-900, Viçosa, Minas Gerais, Brazil; Central Metabolism Group, Max Planck Institute of Molecular Plant Physiology, 14476 Potsdam-Golm, Germany (D.M.D., A.R.F.); and Institute of Plant Biology, University of Zurich, Zollikerstrasse 107, CH–8008 Zürich, Switzerland (E.M.)

ORCID IDs: 0000-0001-9086-730X (D.B.M.); 0000-0002-1136-6564 (J.H.F.C.).

Stomata control the exchange of CO_2 and water vapor in land plants. Thus, whereas a constant supply of CO_2 is required to maintain adequate rates of photosynthesis, the accompanying water losses must be tightly regulated to prevent dehydration and undesired metabolic changes. Accordingly, the uptake or release of ions and metabolites from guard cells is necessary to achieve normal stomatal function. The *AtQUAC1*, an R-type anion channel responsible for the release of malate from guard cells, is essential for efficient stomatal closure. Here, we demonstrate that mutant plants lacking AtQUAC1 accumulated higher levels of malate and fumarate. These mutant plants not only display slower stomatal closure in response to increased CO_2 concentration and dark but are also characterized by improved mesophyll conductance. These responses were accompanied by increases in both photosynthesis and respiration rates, without affecting the activity of photosynthetic and respiratory enzymes and the expression of other transporter genes in guard cells, which ultimately led to improved growth. Collectively, our results highlight that the transport of organic acids plays a key role in plant cell metabolism and demonstrate that AtQUAC1 reduce diffusive limitations to photosynthesis, which, at least partially, explain the observed increments in growth under well-watered conditions.

Stomata are functionally specialized microscopic pores that control the essential exchange of CO_2 and H_2O with the environment in land plants. Stomata are found on the surfaces of the majority of the aerial parts of plants, rendering them as the main control point regulating the flow of gases between plants and their surrounding atmosphere. Accordingly, the majority of water loss from plants occurs through stomatal pores, allowing plant transpiration and CO_2 absorption for the photosynthetic process (Bergmann and Sack, 2007; Kim et al., 2010). The maintenance of an adequate water balance through stomatal control is crucial to plants because cell expansion and growth require tissues to remain turgid (Sablowski and Carnier Dornelas, 2014), and minor reductions in cell water volume and turgor pressure will therefore compromise both processes (Thompson, 2005). As a result, the high sensitivity of plant tissues to turgor has prompted the use of reverse genetic studies in attempt to engineer plants with improved performance (Cowan and Troughton, 1971; Xiong et al., 2009; Borland et al., 2014; Franks et al., 2015).

In most land plants, not only redox signals invoked by shifts in light quality (Busch, 2014) but also the transport of inorganic ions (e.g. K^+, Cl^-, and NO^-_3) as well as metabolites such as the phytohormone abscisic acid (ABA), Suc, and malate, are important players controlling stomatal movements (Hetherington, 2001; Roelfsema and Hedrich, 2005; Pandey et al., 2007; Blatt et al., 2014; Kollist et al., 2014). In this context, although organic acids in plants is known to support numerous

[1] This work was supported by funding from the Max Planck Society (to W.L.A.), the National Council for Scientific and Technological Development (CNPq-Brazil, grant no. 483525/2012-0 to W.L.A.), and the FAPEMIG (Foundation for Research Assistance of the Minas Gerais State, Brazil, grant nos. APQ-01106-13 and APQ-01357-14 to W.L.A.). Scholarships granted by FAPEMIG to D.B.M., CNPq to D.M.D. and S.C.V.M., and Coordination for the Improvement of Higher Level Personnel (CAPES) to J.H.F.C. Fellowships granted by CNPq-Brazil to A.N.N and W.L.A. are gratefully acknowledged.

* Address correspondence to wlaraujo@ufv.br.

The author responsible for distribution of materials integral to the findings presented in this article in accordance with the policy described in the Instructions for Authors (www.plantphysiol.org) is: Wagner L. Araújo (wlaraujo@ufv.br).

D.B.M., A.R.F., and W.L.A. designed the research; D.B.M., S.C.V.M., and J.H.F.C. performed the research; D.M.D., E.M., A.N.N., and F.M.D. contributed new reagents/analytic tools; D.B.M., S.C.V.M., F.M.D., A.R.F., and W.L.A. analyzed the data; and D.B.M., A.R.F., and W.L.A. wrote the article with input from all the others.

www.plantphysiol.org/cgi/doi/10.1104/pp.15.01053

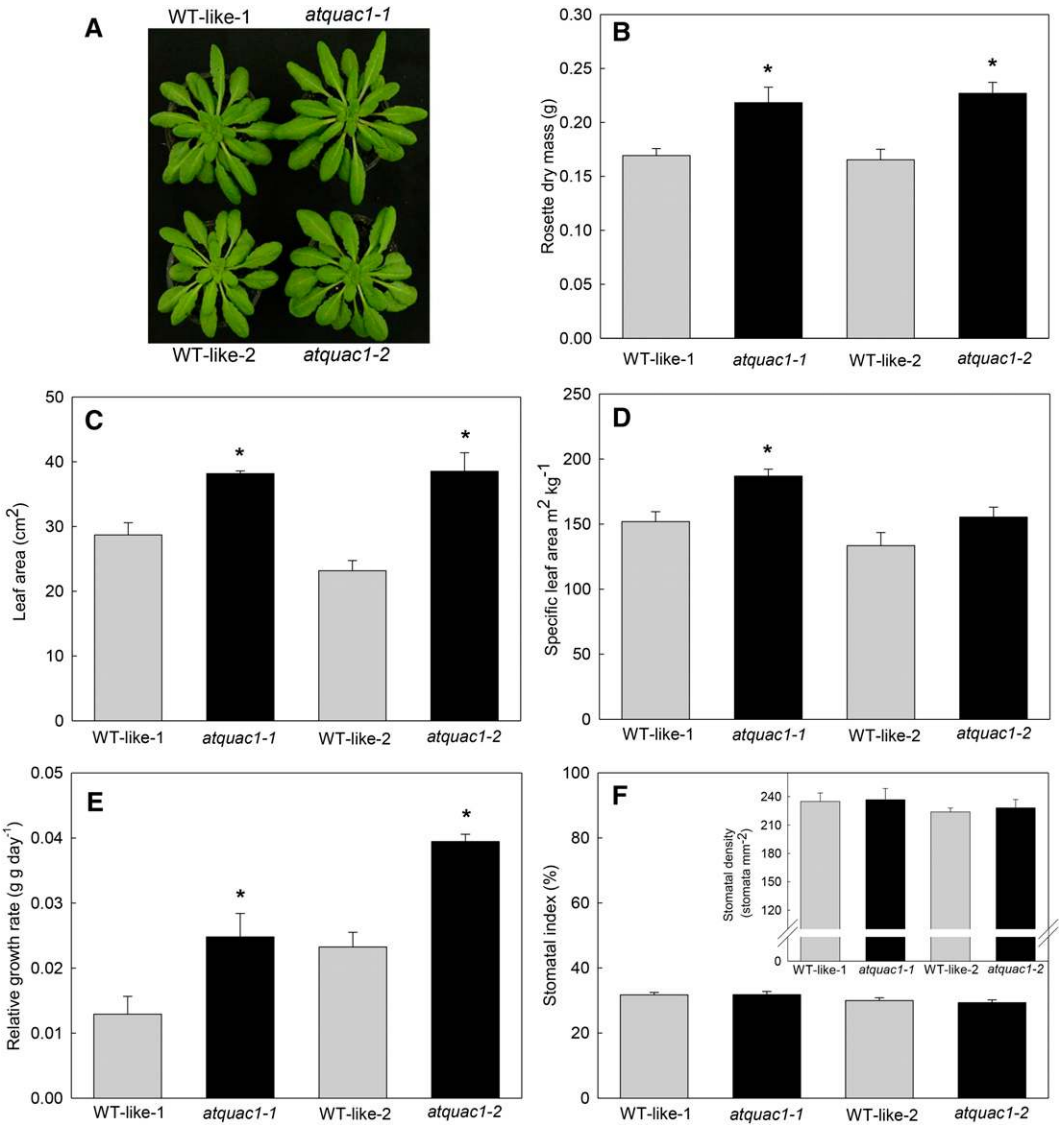

Figure 1. Phenotype, growth, and morphological parameters in WT-like and *atquac1* mutant plants under normal growth conditions. A, Representative images of 5-week-old Arabidopsis plants observed in at least four independent assays. Plants with reduced expression of *AtQUAC1* were compared with plants that genotyped as wild-type (WT-like) during homozygous screening by PCR (for details, see Meyer et al., 2010). In all analyses performed, *atquac1-1* and *atquac1-2* mutant lines were directly compared with the corresponding WT lines (WT-like-1 and WT-like-2, respectively). B, RDM. C, LA. D, SLA. E, RGR. F, Stomatal index and stomatal density. Values are presented as means ± SE ($n = 8$) obtained in two independent assays (four in each assay); values in bold in *atquac1* plants were determined by Student's *t* test to be significantly different ($P < 0.05$) from their corresponding WT-like.

and diverse functions both within and beyond cellular metabolism, only recently have we obtained genetic evidence to support that modulation of guard cell malate and fumarate concentration can greatly influence stomatal movements (Nunes-Nesi et al., 2007; Araújo et al., 2011b; Penfield et al., 2012; Medeiros et al., 2015). Notably malate, in particular, has been considered as a key metabolite and one of the most important organic metabolites involved in guard cell movements (Hedrich and Marten, 1993; Fernie and Martinoia, 2009; Meyer et al., 2010). During stomatal aperture, the flux of malate into guard cells coupled with hexoses generated on starch breakdown lead to decreases in the water potential, and consequently, water uptake by the guard cells ultimately opens the stomata pore (Roelfsema and Hedrich, 2005; Vavasseur and Raghavendra, 2005; Lee et al., 2008). On the other hand, during stomatal closure, malate is believed to be converted into starch, which has no osmotic activity (Penfield et al., 2012) or, alternatively, is released from the guard cells to the surrounding apoplastic space (Lee et al., 2008; Negi et al., 2008; Vahisalu et al., 2008; Meyer et al., 2010).

The role of organic acids on the stomatal movements has been largely demonstrated by studies related to

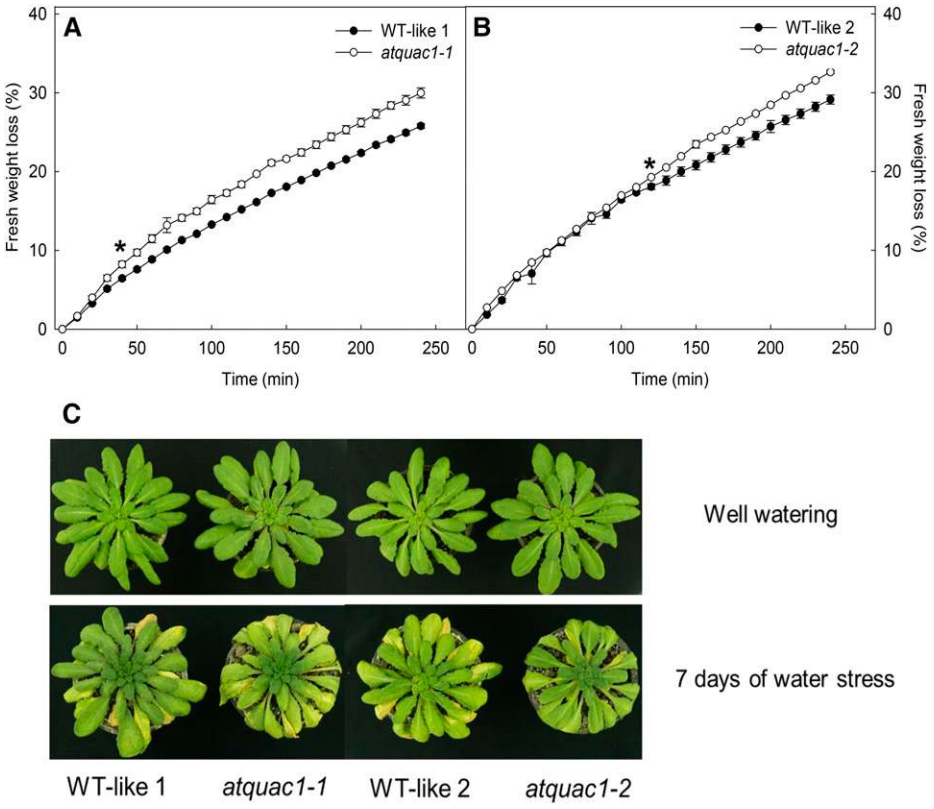

Figure 2. *atquac1* mutant plants lost water faster than WT-like plants. A and B, Fresh weight loss from detached whole rosettes in WT-like-1 and *atquac1-1* (A) and WT-like-2 and *atquac1-2* (B), respectively. Data show percentage of initial fresh weight loss from detached rosettes incubated under the same plant growth conditions. Values are presented as means ± SE (n = 8) obtained in two independent assays. Asterisk indicates that from this point and above, the values from mutant lines were determined by Student's t test to be significantly different ($P < 0.05$) from its corresponding WT-like. C, Phenotype of 5-week-old, short-day-grown Arabidopsis mutants and wild-type plants (WT) 7 d after water limitation. *atquac1* plants are more sensitive to drought; 7 d after stopping watering (bottom panel), WT-like plants are still turgid while the corresponding *atquac1* plants are mostly dehydrated.

malate transport (Lee et al., 2008; Meyer et al., 2010; Sasaki et al., 2010). In the last decade, two protein families were identified and functionally characterized to be directly involved with organic acid transport at the guard cell plasma membrane and to be required for stomatal functioning (Lee et al., 2008; Meyer et al., 2010; Sasaki et al., 2010). In summary, AtABCB14, a member of the ABC (ATP binding cassette) family, which is involved in malate transport from apoplast to guard cells, was described as a negative modulator of stomatal closure induced by high CO_2 concentration; notably, exogenous application of malate minimizes this response (Lee et al., 2008). In addition, members of a small gene family, which encode the anion channels SLAC1 (slow anion channel 1) and four SLAC1-homologs (SLAHs) in Arabidopsis (*Arabidopsis thaliana*), have been described to be involved in stomatal movements. SLAC1 is a well-documented S-type anion channel that preferentially transports chloride and nitrate as opposed to malate (Vahisalu et al., 2008, 2010; Geiger et al., 2010; Du et al., 2011; Brandt et al., 2012; Kusumi et al., 2012). Lack of SLAC1 in Arabidopsis and rice (*Oryza sativa*) culminated in a failure in stomatal closure in response to high CO_2 levels, low relative humidity, and dark conditions (Negi et al., 2008; Vahisalu et al., 2008; Kusumi et al., 2012). Although mutations in AtSLAC1 impair S-type anion channel functions as a whole, the R-type anion channel remained functional (Vahisalu et al., 2008). Indeed, a member of the aluminum-activated malate transporter (ALMT) family, AtALMT12, an R-type anion channel, has been demonstrated to be involved in malate transport, particularly at the plasma membrane of guard cells (Meyer et al., 2010; Sasaki et al., 2010). Although AtALMT12 is a member of ALMT family, it is not activated by aluminum, and therefore Meyer et al. (2010) proposed to rename it as AtQUAC1 (quick-activating anion channel 1; Imes et al., 2013; Mumm et al., 2013). Hereafter, we will follow this nomenclature. Deficiency of a functional AtQUAC1 has been documented to lead to changes in stomatal closure in response to high levels of CO_2, dark, and ABA (Meyer et al., 2010). Taken together, these studies have clearly demonstrated that both S- and R-type anion channels are key modulators of stomatal movements in response to several environmental factors.

Despite a vast number of studies involving the above-mentioned anion channels, little information concerning the metabolic changes caused by their impairment is currently available. Such information is important to understand stomatal movements, mainly considering that organic acids, especially the levels of malate in apoplastic/mesophyll cells, have been highlighted as of key importance in leaf metabolism (Fernie and Martinoia, 2009; Araújo et al., 2011a, 2011b; Lawson et al., 2014; Medeiros et al., 2015). Here, we demonstrate that a disruption in the expression of *AtQUAC1*, which leads to impaired stomatal closure (Meyer et al., 2010), was accompanied by increases in mesophyll conductance (g_m), which is defined as the conductance for the transfer of CO_2 from the intercellular airspaces (C_i) to the sites of carboxylation in the chloroplastic stroma (C_c). By further

Table I. *Gas exchange and chlorophyll a fluorescence parameters in WT-like and atquac1 plants*

Values are presented as means ± SE (n = 10) obtained using the ninth leaf totally expanded from 10 different plants per genotype in two independent assays (five plants in each assay). Values in bold in *atquac1* plants were determined by Student's t test to be significantly different ($P < 0.05$) from its corresponding WT-like.

Parameters[a]	WT-Like-1	*atquac1-1*	WT-Like-2	*atquac1-2*
A_N (μmol CO_2 m^{-2} s^{-1})	6.23 ± 0.49	**8.74 ± 0.20**	6.53 ± 0.30	**7.65 ± 0.35**
g_s (mol H_2O m^{-2} s^{-1})	0.15 ± 0.03	**0.22 ± 0.01**	0.15 ± 0.01	**0.20 ± 0.02**
WUEi (A_N/g_s)	41.0 ± 5.5	40.7 ± 1.2	41.1 ± 3.0	40.3 ± 3.3
R_d (μmol CO_2 m^{-2} s^{-1})	0.85 ± 0.10	**1.29 ± 0.17**	0.66 ± 0.14	**1.28 ± 0.13**
F_v/F_m	0.79 ± 0.01	0.78 ± 0.02	0.77 ± 0.03	0.78 ± 0.01
F_v'/F_m'	0.57 ± 0.007	0.58 ± 0.007	0.56 ± 0.006	0.57 ± 0.005
J_{flu} (μmol m^{-2} s^{-1})	70.8 ± 2.12	**79.8 ± 1.8**	71.0 ± 4.4	75.7 ± 2.6

[a]A_N, Net photosynthesis rate; g_s, stomatal conductance; *WUEi*, intrinsic water use efficiency; F_v/F_m, maximum PSII photochemical efficiency; F_v'/F_m', actual PSII photochemical efficiency; J_{flu}, electron transport rate estimated by chlorophyll fluorescence parameters.

characterization of *atquac1* knockout plants, we demonstrated that reduced diffusive limitations resulted in higher photosynthetic rates and altered respiration that, in turn, led to enhanced biomass accumulation. Overall, the results obtained are discussed both in terms of the importance of organic acid transport in plant cell metabolism and with regard to the contribution that it plays in the regulation of both stomatal function and growth.

RESULTS

atquac1 Plants Exhibited Slightly Elevated Leaf Growth

Given that stomata are the main gate to control CO_2 influx into leaves, we investigated whether mutations in *AtQUAC1* affected growth parameters in the two independent *atquac1* T-DNA lines (*atquac1-1* and *atquac1-2*) described in detail by Meyer et al. (2010). We first confirmed the absence of *AtQUAC1* transcripts in leaves of the mutants by reverse transcription PCR (Supplemental Fig. S1). The mutant lines, which had no visible aberrant phenotypes during the vegetative growth phase (Fig. 1A), displayed enhanced rosette dry mass (Fig. 1B) and relative growth rate (RGR; Fig. 1E), coupled with increased total leaf area (LA; Fig. 1C) and specific leaf area (SLA; Fig. 1D). Although we observed clear differences between the two mutant lines in their RGR, when compared to their respective WT-like (for genotyped as wild type) plants, we noticed that the enhancement observed in RGR was proportionally similar between *atquac1* T-DNA lines. We additionally observed that stomatal density and stomatal index (Fig. 1F) were unaltered in both mutant lines.

Closing Kinetics, Water Loss, and Sensitivity to Drought Are Affected in *atquac1* plants

The absence of AtQUAC1 has been previously demonstrated to impact stomatal closure in response to both CO_2, dark, and ABA (Meyer et al., 2010). To further assess the impact of the lack of a functional AtQUAC1 on stomatal conductance (g_s) and water loss in Arabidopsis plants, we next adopted three complementary approaches. First, we confirmed the duration of stomatal responses following dark-to-light and light-to-dark transitions as well as normal-to-high and high-to-normal CO_2 concentrations (Supplemental Fig. S2). Our results confirmed the deficient stomatal regulation in mutant plants, which showed slower stomatal closing kinetics in response to both light-to-dark transitions (Supplemental Fig. S2, A and B) and normal-to-high CO_2 concentrations (Supplemental Fig. S2, C and D). In contrast, the light-stimulated opening kinetics was less affected, albeit we also observed a relative tendency of faster opening and higher g_s, even in response to high CO_2 levels. Given that *atquac1* plants have slower stomatal closing, despite similar stomatal density (Fig. 1F), we next performed a time scale water loss experiment from excised rosettes by analyzing fresh weight loss. Consistent with slower stomatal closure, water loss was similar in both WT-like and *atquac1* plants during the beginning of the experiment. However, after 240 min, water loss from *atquac1* plants resulted in 32% fresh weight loss against 28% in WT-like plants (Fig. 2, A and B). These data suggest that *atquac1* plants most likely exhibit higher sensitivity to stress conditions. However, given that fresh weight loss in the detached rosette might not reflect the situation *in planta*, we next decided to analyze the response of those plants following water restriction in plants growing on soil. Indeed, after suspension of irrigation, *atquac1* plants showed earlier symptoms of chlorosis and leaf wilting, i.e. 4 to 5 d after withholding watering against 6 to 7 d in both WT-like plants (Fig. 2C). Thus, absence of *AtQUAC1* in Arabidopsis plants is likely to increase its sensitivity to drought episodes.

AtQUAC1 Deficiency Results in Increased g_m and Enhanced Photosynthesis Rate

Considering that most of plant biomass is derived from photosynthesis, we fully characterized the

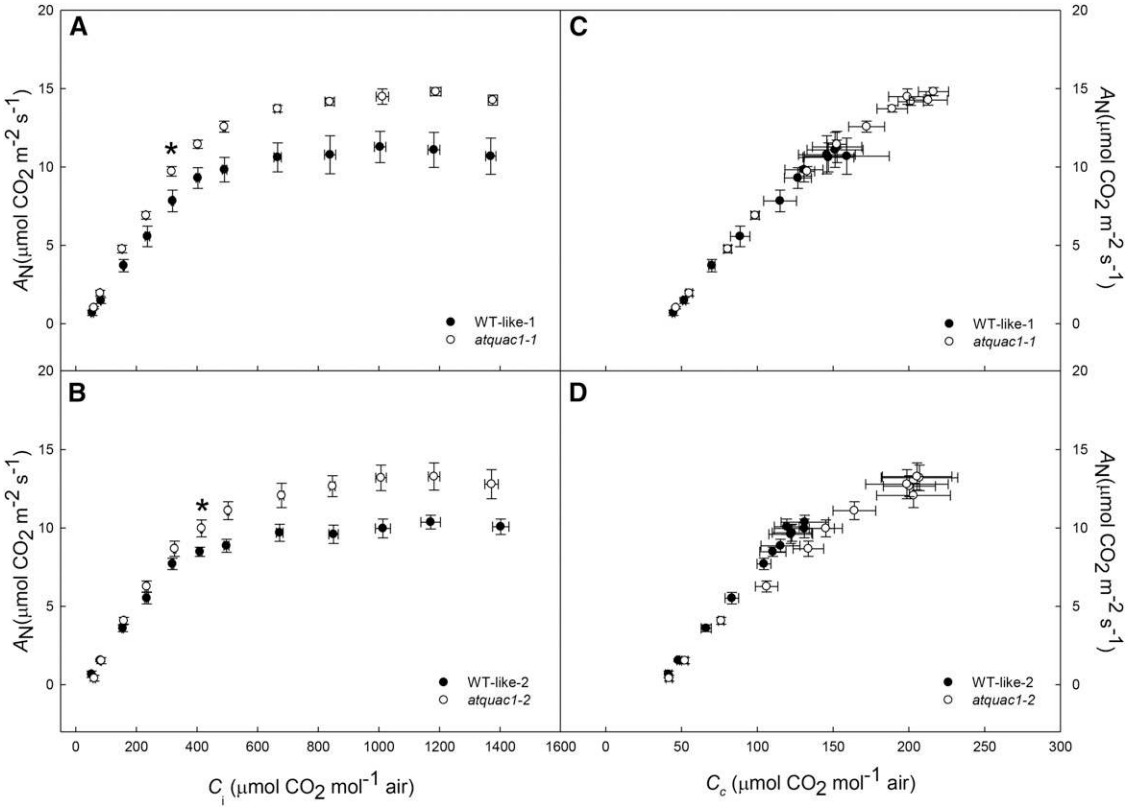

Figure 3. Net photosynthesis (A_N) curves in response to substomatal (C_i) or chloroplastic (C_c) CO_2 concentrations in WT-like and *atquac1* plants. A to D, A_N/C_i curves (A and B) and A_N/C_c curves (C and D) to WT-like-1/*atquac1-1* and WT-like-2/*atquac1-2*, respectively. Asterisk indicates that from this point and above, the A_N in *atquac1* plants were statistically higher than WT-like ones by Student's *t* test ($P < 0.05$). Values are presented as means ± SE ($n = 10$) obtained using the ninth leaf totally expanded from ten different plants per genotype in two independent assays (five plants in each assay).

photosynthetic performance by analyzing diffusional, photochemical, and biochemical constraints to photosynthesis. Compared with their respective WT control, mutant plants displayed higher net photosynthetic rates (A_N) and g_s whereas no differences in intrinsic water use efficiency (*WUEi*) were observed (Table I). Dark respiration (R_d) was higher (approximately 40%) in *atquac1* plants than in their respective WT-like counterparts (Table I). The differences in A_N were unlikely to have been related to photochemical constraints given that both the maximum quantum efficiency of photosystem II (PSII; F_v/F_m) and capture efficiency of excitation energy (F_v'/F_m') remained invariant. Additionally, the electron transport rate (J_{flu}) was marginally increased only in *atquac1-1* (Table I).

By further analyzing gas exchange under photosynthetically active photon flux density (PPFD) that ranged from 0 to 1000 μmol m^{-2} s^{-1}, we observed that mutant plants exhibited unaltered A_N irrespective of the irradiance. Indeed, the saturation irradiance (I_s) and the light-saturated A_N (A_{PPFD}) were increased only in *atquac1-2* plants with no changes both in the compensation irradiance (I_c) and light use efficiency (Supplemental Table S1; Supplemental Fig. S3). Additionally, the response of A_N to the internal CO_2 concentration (A_N/C_i curves; Fig. 3, A and B) was obtained, which were further converted into responses of A_N to chloroplastidic CO_2 concentration (A_N/C_c curves; Fig. 3, C and D). Interestingly, under ambient CO_2 concentration (400 μmol mol^{-1}), C_i estimations were similar between *atquac1* and WT-like plants, whereas C_c was increased in *atquac1* plants (Table II). g_m, estimated using a combination of gas exchange and chlorophyll *a* fluorescence parameters via two independent methods, was significantly higher (29%) in *atquac1* plants in comparison to their respective WT-like (Table II). In addition, the maximum carboxylation velocity (V_{cmax}) and maximum capacity for electron transport rate (J_{max}) were higher in both mutant lines only when estimated on a C_i basis, whereas on a C_c basis J_{max} was increased only in *atquac1-1* line (Table II). Moreover, the similarities in the J_{max}:V_{cmax} ratios suggest that although differences in A_N were observed an adequate functional balance between carboxylation and electron transport rates probably occurred.

The overall photosynthetic limitations were next partitioned into their functional components: stomatal

Table II. *Photosynthetic characterization of WT-like and atquac1 plants*

Values are presented as means ± SE (n = 10) obtained using the ninth leaf totally expanded from 10 different plants per genotype in two independent assays (five plants in each assay). Values in bold in *atquac1* plants were determined by Student's t test to be significantly different ($P < 0.05$) from their corresponding WT-like.

Parameters[a]	WT-Like-1	*atquac1-1*	WT-Like-2	*atquac1-2*
C_i (μmol CO_2 mol^{-1})	317.4 ± 7.9	319.4 ± 2.4	315.7 ± 7.4	324.5 ± 6.2
C_c (μmol CO_2 mol^{-1})	100.1 ± 7.3	**133.1 ± 3.76**	104.4 ± 5.0	**133.7 ± 11.0**
g_{m_Harley} (mol CO_2 m^{-2} s^{-1} bar^{-1})	0.029 ± 0.005	**0.043 ± 0.002**	0.030 ± 0.003	**0.042 ± 0.004**
g_{m_Ethier} (mol CO_2 m^{-2} s^{-1} bar^{-1})	0.035 ± 0.005	**0.049 ± 0.002**	0.031 ± 0.003	**0.043 ± 0.004**
$V_{cmax-Ci}$ (μmol m^{-2} s^{-1})	26.8 ± 2.3	**35.9 ± 0.9**	26.4 ± 1.8	**32.2 ± 1.2**
$V_{cmax-Cc}$ (μmol m^{-2} s^{-1})	81.6 ± 1.9	84.8 ± 1.4	81.5 ± 7.1	82.8 ± 6.0
J_{max_Ci} (μmol m^{-2} s^{-1})	53.3 ± 4.1	**81.2 ± 0.7**	55.6 ± 2.9	**74.8 ± 4.1**
J_{max_Cc} (μmol m^{-2} s^{-1})	103.5 ± 3.3	**117.1 ± 1.2**	106.8 ± 7.1	106.7 ± 5.1
J_{max_Ci}: $V_{cmax-Ci}$	2.2 ± 0.10	2.3 ± 0.06	2.1 ± 0.10	**2.3 ± 0.09**
J_{max_Cc}: $V_{cmax-Cc}$	1.2 ± 0.05	1.4 ± 0.02	1.3 ± 0.03	**1.3 ± 0.05**
Stomatal limitation	0.197 ± 0.023	0.197 ± 0.007	0.197 ± 0.020	0.182 ± 0.020
Mesophyll limitation	0.646 ± 0.026	**0.561 ± 0.013**	0.642 ± 0.034	**0.529 ± 0.033**
Biochemical limitation	0.157 ± 0.030	**0.242 ± 0.011**	0.160 ± 0.019	**0.289 ± 0.039**

[a] C_i, Substomatal CO_2 concentration; C_c, chloroplastic CO_2 concentration; g_m, mesophyll conductance to CO_2 estimated according to the Harley or Ethier method; $V_{cmax-Ci\ or\ Cc}$, maximum carboxylation capacity based on C_i or C_c; $J_{max\_Ci\ or\ Cc}$, maximum capacity for electron transport rate based on C_i or C_c.

(l_s), mesophyll (l_m), and biochemical (l_b; Table II). The photosynthetic rates were mainly constrained by l_m (64% and 54% in WT-like and *atquac1* plants, respectively), whereas l_s accounted for, on average, 19% in both WT-like and *atquac1* plants, and l_b contributed with 16% and 26% in WT-like and *atquac1* plants, respectively. These analyses demonstrated that *atquac1* plants exhibits lower l_m compared to the WT-like plants in close agreement with the higher g_m observed (Table II).

Mutations in *AtQUAC1* Affect Mainly Carbon Metabolism without Strong Effects in Activity of Related Enzymes

To explore the consequences of changes in photosynthetic capacity among the genotypes, we further conducted a detailed metabolic analysis in leaves of the mutants and WT-like plants. Evaluation of compounds related to nitrogen metabolism revealed that there were no changes in the levels of nitrate, chlorophylls, total amino acids, and soluble proteins in a consistent manner with the altered expression of *AtQUAC1* (Supplemental Figs. S4 and S5). During the light period, mutant lines accumulated more Glc (Fig. 4, A and B), Suc (Fig. 4, E and F), and starch (Fig. 4, G and H), reaching higher values at the end of this period. Notably, the mutant lines were able to fully degrade these metabolites by the end of the dark period, reaching similar values to those observed in WT-like plants (Fig. 4), corroborating the increased R_d observed in *atquac1* plants (Table I). Suc was the main storage sugar in all genotypes reaching, on average, 3 and 15 times higher contents than those of Glc and Fru, respectively. It is important to note that the higher concentrations of starch and sugars observed in *atquac1* plants were accompanied by higher A_N.

Diel changes in the levels of organic acids (malate and fumarate) were similar to those observed for sugars and starch, with higher values being consistently observed in mutant plants. Remarkably, *atquac1* plants showed increases in both malate and fumarate content mainly at the middle of the light period (Fig. 5; Supplemental Fig. S3).

We next decided to extend this study to major primary pathways of plant photosynthetic metabolism by using an established gas chromatography-mass spectrometry (GC-MS) protocol (Lisec et al., 2006). This analysis revealed, however, that among the 40 successfully annotated compounds related to primary metabolism, only a relatively small number of changes were evident (Fig. 5). By analyzing 13 individual amino acids, we observed increases only in Gln, Pro, Gly, and Ala, which were moreover only significantly different in *atquac1-1* plants (Fig. 5). When considering the levels of the organic acids, we also observed that only the levels of maleic acid, malate, fumarate, succinate (only in *atquac1-1*), and glycerate (only in *atquac1-2*) increased in mutant lines. Other changes of note in the metabolite profiles were the significant increases in glycerol and myoinositol (in both lines, Fig. 5).

We next investigated whether the metabolic perturbation observed could also affect the activity of important enzymes related to photosynthetic and respiratory metabolism (Table III). Although changes in both photosynthesis and respiration were observed in *atquac1* plants, there were no changes in either Rubisco or NADP-dependent malate dehydrogenase (NADP-MDH). Moreover, increases in transketolase activity were observed in both *atquac1* lines, whereas glyceraldehyde 3-phosphate dehydrogenase (GAPDH)

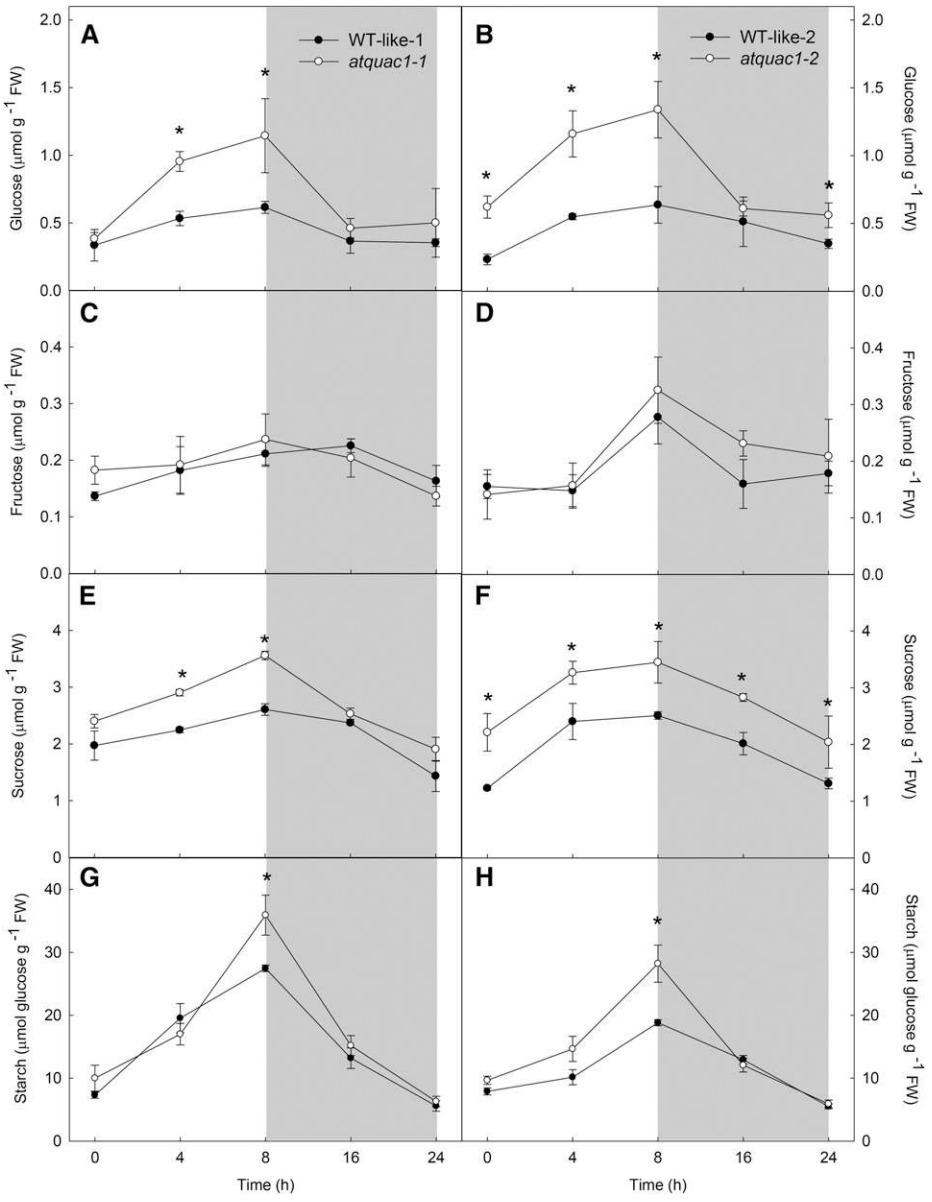

Figure 4. Leaf metabolite levels in WT-like and *atquac1* plants. A and B, Glc; C and D, Fru; E and F, Suc; G and H, starch to WT-like-1 and *atquac1-1* as well as WT-like-2 and *atquac1-2*, respectively. Values are presented as means ± SE (n = 5) from whole rosettes harvested in different times along the cycle of light/dark. Asterisks indicate the time where the values from mutant lines were determined by Student's t test to be significantly different ($P < 0.05$) from their corresponding WT-like.

activity was increased only in *atquac1-1* plants. Regarding enzymes related to respiratory metabolism, no significant changes were observed for the activities of Suc synthase (Susy), phosphoglycerate kinase (PGK), or NAD-dependent malate dehydrogenase (NAD-MDH).

AtQUAC1 Repression Does Not Strongly Affect the Expression of Other Genes Related to Ion Transport in Guard Cells

We next analyzed whether *AtQUAC1* repression affected the expression of genes currently known to or putatively related to organic and inorganic ion transport, as well as genes involved in guard cell movements. We felt such experiments were important given that the loss of function of *AtSLAC1* was associated with downregulation of several guard-cell-expressed transporters (Laanemets et al., 2013). To extend this molecular characterization, we attempted to look at the expression levels of several ion channels and transporter in guard cells from isolated epidermal fragments, including *ALMT6*, *ALMT9*, *AtABCB14*, *AtSLAC1*, *AHA1*, *AHA5*, *KAT1*, *KAT2*, *AKT1*, *AKT2*, *AtKC1*, *TPC1*, and *GORK* (for further details, see "Materials and Methods" and Supplemental Table S2). Quantitative real-time PCR (qRT-PCR) analysis of the transcript levels of these genes revealed, in sharp contrast to the situation observed in the case of *atslac1* plants (Laanemets et al., 2013), that the vast majority of evaluated genes in *atquac1* plants were unaltered

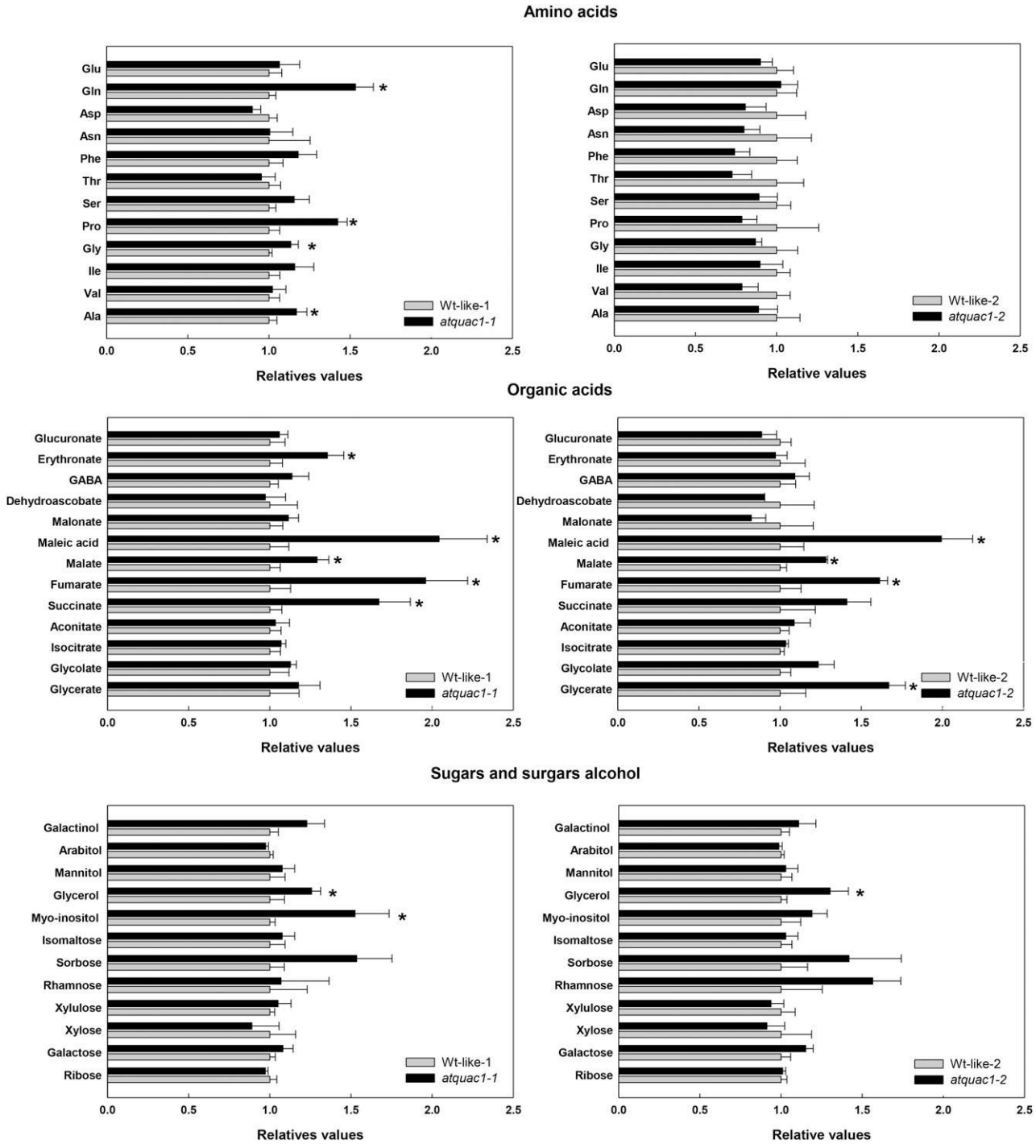

Figure 5. Relative metabolite content in leaves of WT-like and *atquac1* plants. Amino acids, organic acids, and sugars and sugar-alcohols were determined by GC-MS as described in "Materials and Methods." The full data sets from these metabolic profiling studies are additionally available in Supplemental Table S3. Data are normalized with respect to the mean response calculated for the corresponding WT-like (to allow statistical assessment, individual plants from this set were normalized in the same way). WT-like-1 or -2, Gray bars; *atquac1-1* or *-2*, black bars. Values are presented as means ± SE ($n = 5$). Asterisks indicate that the values from mutant lines were determined by Student's *t* test to be significantly different ($P < 0.05$) from their corresponding WT-like.

(Fig. 6). Thus, although *KAT1* and *KAT2* were reduced in *atquac1-2* plants only and the *AHA5* transcript level was increased in *atquac1-1* plants only, our results indicate that the stomatal effects observed here were not likely to be mediated by an alteration in the general efficiency of transport of the guard cells.

Table III. *Enzyme activities in WT-like and atquac1 plants*

Activities were determined in whole rosettes (5-week-old) harvested at middle of the photoperiod. Values are presented as means ± SE ($n = 5$); values in bold type in *atquac1* plants were determined by Student's *t* test to be significantly different ($P < 0.05$) from their corresponding WT-like. FW, Fresh weight.

Enzymes	WT-Like-1	*atquac1-1*	WT-Like-2	*atquac1-2*
	nmol min^{-1} g^{-1} FW			
Rubisco initial	946.4 ± 69.2	1078.0 ± 105.2	909.3 ± 77.8	896.8 ± 112.6
Rubisco total	1450.9 ± 71.3	1629.5 ± 24.7	1229.7 ± 93.3	1396.4 ± 66.7
Rubisco activation state[a]	66.7 ± 1.9	66.5 ± 7.4	68.0 ± 3.1	68.9 ± 2.7
Transketolase	303.8 ± 13.9	**404.9 ± 8.9**	299.4 ± 15.4	**347.9 ± 12.3**
NADP-GAPDH	37.3 ± 1.7	**74.0 ± 1.8**	46.4 ± 3.8	44.7 ± 0.7
NADP-MDH initial	39.0 ± 1.7	40.6 ± 2.4	33.0 ± 1.6	32.3 ± 2.3
NADP-MDH total	63.8 ± 4.5	65.9 ± 4.2	62.9 ± 2.4	61.4 ± 3.9
NADP-MDH activation state[a]	62.1 ± 3.9	58.8 ± 5.8	51.9 ± 2.9	48.7 ± 4.7
Susy	512.7 ± 15.9	548.4 ± 22.9	458.1 ± 19.4	444.9 ± 3.4
PGK[b]	12.5 ± 0.4	13.8 ± 0.6	11.6 ± 0.6	12.6 ± 0.5
NAD-MDH[b]	24.7 ± 0.7	27.0 ± 0.9	25.5 ± 0.8	27.0 ± 0.6

[a]Activation state expressed in percentage (%). [b]Values expressed in μmol min^{-1} g^{-1} fresh weight.

DISCUSSION

Ion transport from guard cells to their surroundings has been proven essential to stomatal movements. Indeed, it is well known that the efflux of malate from guard cells can regulate the activity of anion channels on guard cell membrane (Hedrich and Marten, 1993; Hedrich et al., 1994; Raschke, 2003; Lee et al., 2008; Negi et al., 2008; Kim et al., 2010), suggesting that the organic acid accumulation on the apoplast space might influence stomatal movements. Indeed, the role of the organic acids (e.g. malate and fumarate) on the regulation of stomata movements was recently confirmed (Nunes-Nesi et al., 2007; Meyer et al., 2010; Araújo et al., 2011b; Medeiros et al., 2015). However, the metabolic hierarchy regulating those highly specialized cell types, as yet, remains elusive. Here, by using a combination of physiological and biochemical approaches, we provide evidence that the genetic manipulation of organic acid transport has significant potential to biotechnological applications (Martinoia et al., 2012; Schroeder et al., 2013; Medeiros et al., 2015). Both the data we provide and the recent molecular characterization of Arabidopsis plants deficient in the expression of *AtQUAC1* (Meyer et al., 2010; Sasaki et al., 2010) and data concerning the regulation of AtQUAC1 (Imes et al., 2013; Mumm et al., 2013) add further support to the importance of this anion channel regulating stomatal movements. Importantly, we showed that other aspects of photosynthetic and respiratory metabolism, the GC-MS-based metabolite profile (Fig. 5; Supplemental Table S3), and the transcript levels of some key channels and transporters involved in guard cell ion transport (Fig. 6) all displayed relatively few and mild changes. Such observations likely indicate that AtQUAC1 plays little part in terms of total cellular homeostasis. It is important to note here that impairments in the AtSLAC1 activity also reduced stomatal opening kinetics that were associated not only with the repression of an organic acid transporter (reduction in *AtABCB14* expression), but mainly due the dramatic reductions of inward K^+ channel currents (Laanemets et al., 2013). In this study, the authors also identified a compensatory feedback control in *atslac1* plants involving the elevation of cytosolic Ca^{2+} concentrations, which downregulated the inward K^+ channel activity. By contrast, stomatal opening kinetics were not significantly altered in *atquac1* plants (Supplemental Fig. S2). Furthermore, as changes in the activities of key enzymes of photosynthetic and respiratory metabolism were not observed (Table III) and V_{cmax} on a C_c basis (Table II) was similar between WT-like and *atquac1* plants, we contend that diffusive rather than biochemical limitations had a major role explaining the changes in photosynthetic rates. These results, coupled with those obtained by Meyer et al. (2010) and Sasaki et al. (2010), provide strong evidence that AtQUAC1 is essential for an efficient stomatal closure yet does not strongly affect the central primary metabolism.

Functional Absence of AtQUAC1 Alters Stomatal Movements and Mesophyll Conductance

Given the increased photosynthetic rates and subsequent increases in LA and RGR (Figs. 1 and 3; Table I), we next investigated the mechanisms underlying this positive growth response. Since the changes described above took place independently of changes in the stomatal density and photosynthetic pigment levels (Fig. 1F; Supplemental Fig. S4), it is reasonable to assume that molecular and metabolic mechanisms occurred enabling a reprogramming in response to impaired stomatal closure in *atquac1* plants under our experimental conditions. The results presented here provide further evidence that the functional lack of AtQUAC1 leads to slower stomatal closure in response to dark and high CO_2 concentrations (Supplemental Fig. S2). Additional compelling evidence supporting the role of AtQUAC1 on the regulation of stomatal function was

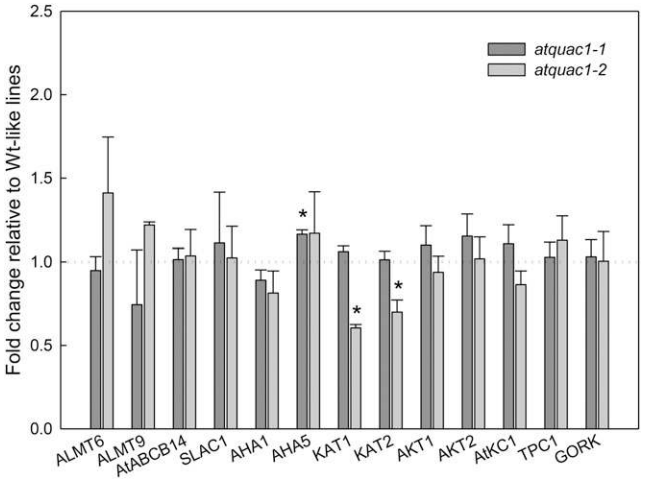

Figure 6. Relative transcript responses of genes involved in organic and inorganic ion transport in guard cell. Transcript abundance of Arabidopsis plasma membrane H^+-ATPases *AHA1* and *AHA5*, transporter *AtABCB14*, and ion channels *ALMT6*, *ALMT9*, *SLAC1*, *KAT1*, *KAT2*, *AKT1*, *AKT2*, *TPC1*, *AtKC1*, and *GORK* was determined. RNA was isolated from epidermal fragments. Data are normalized with respect to the mean response calculated for the corresponding WT-like. *atquac1-1*, Black bars; *atquac1-2*, gray bars. Values are presented as means ± SE ($n = 4$); asterisks indicate values that were determined by Student's *t* test to be significantly different ($P < 0.05$) from their corresponding WT-like.

further obtained from assays of fresh weight water loss and drought stress (Fig. 2). Collectively, these analyses showed that the mutant lines lost water faster than their respective WT-like, characterizing a water-spending phenotype and likely more sensitive to drought events (Fig. 2C). Thus, these data clearly document the importance of AtQUAC1 and, by extension, organic acid transport in guard cell function.

Plant photosynthetic capacity was considered for a long time to be limited only by the rate of CO_2 diffusion through the stomata and by the capability of the photosynthetic machinery to convert the light energy into biochemical one (Flexas et al., 2012). However, it is now recognized that the pathway to CO_2 diffusion from stomata to the Rubisco carboxylation sites in the chloroplasts can become an important limiting factor to the photosynthetic process due to the several resistances in the gas and liquid phases during this way. Thus, g_m, previously considered large enough to have any impact on photosynthesis (Farquhar et al., 1980), has recently turned out to be a key point in explaining limitations during this process (Bernacchi et al., 2002; Flexas et al., 2007, 2012, 2013; Warren, 2008b; Bown et al., 2009; Niinemets et al., 2009; Jin et al., 2011; Scafaro et al., 2011; Martins et al., 2013). Noteworthy, g_s and g_m are very often coregulated (Flexas et al., 2012), which can reflect either a strong coordination between A_N and g_s or a compensatory mechanism, where g_m tends to compensate changes in g_s particularly under suboptimal conditions (e.g. drought). In such cases, where g_s seems to be more affected than g_m, this coregulation has the purpose of optimizing A_N (Warren, 2008a; Duan et al., 2009; Vrábl et al., 2009; Galmés et al., 2011; Flexas et al., 2012; Galmés et al., 2013). Accordingly, photosynthetic limitations were estimated and revealed that the mesophyll fraction had a greater contribution to the lower A_N observed in WT-like compared to *atquac1* plants (Table II). Collectively, the results presented here demonstrate that the higher capacity of CO_2 fixation in *atquac1* plants was associated with a higher C_c due to increased g_m in *atquac1* mutant plants that can, at least partially, explain the increased growth presented by those plants (Fig. 1). The observed effects on g_s, which were followed by increases in g_m (Tables I and II) without changes in the stomatal density (Fig. 1F), indicate that the diffusional component was the main player controlling A_N. Detailed biochemical and physiological analyses delimited this response as a consequence of perturbation of stomatal function; however, the exact mechanisms underlying this phenomenon are not immediately evident. Although several studies have attempted to explain both stomata physiology and variations in g_m (Kollist et al., 2014; Lawson et al., 2014), which may rely on anatomical properties (Peguero-Pina et al., 2012), our understanding of this subject remains far from complete. Accordingly, a parameter commonly used to characterize the physical limitation inside the leaves is the leaf dry mass per unit area (LMA) that increase as a function of increases in cell wall thickness, potentially decreasing the velocity of CO_2 diffusion (Flexas et al., 2008; Niinemets et al., 2009; Flexas et al., 2012). The LMA is considered a key trait in plant growth and performance, allowing plants to cope with different environmental conditions most likely because the amount of light absorbed by a leaf and the diffusion pathway of CO_2 through the leaf depend partially on its thickness (Vile et al., 2005; Poorter et al., 2009, Villar et al., 2013). The inverse of LMA is the ratio of leaf area to leaf mass or SLA; thus, a reduction in LMA is translated into increments in SLA and, in turn, increases in g_m. Indeed, the values of SLA found here are in agreement with this hypothesis once we observed higher values of both SLA and g_m in *atquac1* plants (Fig. 1D; Table II). In this vein, although we have not observed changes in stomatal density but increased SLA, studies related to the leaf anatomy of these mutants might help to explain whether the increases in g_m are governed by anatomic traits or by further investments of nitrogen to mesophyll proteins involved in increasing g_m, such as carbonic anhydrases, aquaporins, Rubisco, and others (Buckley and Warren, 2014). Accordingly, it is not without precedence to suggest that changes in g_m will eventually correlate with changes in sugars, which are cell wall precursors, and, to a lower extent, to organic acids, as observed here. In this sense, it seems plausible that an interaction between these compounds may exist and, thus, directly or indirectly be associated with enhancement of g_m, and by extension A_N. It will be important to establish the functional significance of this observation in future studies.

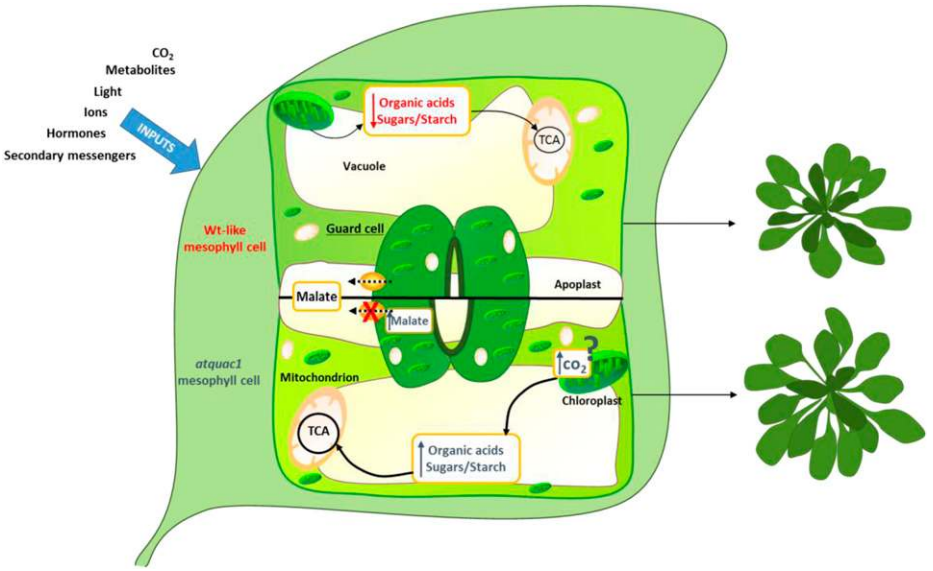

Figure 7. Hypothetical model connecting the malate accumulation and stomatal movements. The functional lack of *AtQUAC1* is most likely associated with an accumulation of malate inside guard cells, which consequently maintains stomatal pore aperture for a longer time. Although photosynthetic rates are increased through a mechanism not yet fully understood, this is likely related to the maintenance of a high chloroplastic CO_2 concentration given that mesophyll conductance is also increased. Moreover, carbon balance and metabolism are changed through increased levels of sugars, starch, organic acids, and dark respiration rates. Altogether, increased respiration, carbohydrate pool, and photosynthesis can partially explain the observed growth enhancement in *atquac1* plants.

Carbon Metabolism Is Changed as Consequence of the Higher Photosynthetic Rates in *atquac1* Plants

The organic acid levels in the apoplast exhibited a negative correlation between the malate and fumarate content and g_s, with a greater contribution of malate (Nunes-Nesi et al., 2007; Araújo et al., 2011b). This information, coupled to the results obtained with the malate transporter AtABCB14 (Lee et al., 2008), provides strong evidence that the apoplastic content of malate and fumarate can modulate the functioning of guard cells and, in turn, affect the stomatal movements with effects on leaf metabolism. The results presented here demonstrate that impaired organic acid transport, which culminates with alteration in g_s and g_m, promote minor changes in primary metabolism, mainly in carbon metabolism, under normal growth conditions. This fact notwithstanding, the increases in the hexose contents in *atquac1* plants were observed not to be primarily due to increases in Suc or starch breakdown since these metabolites accumulated over the course of the light period (Fig. 4). In good agreement with the higher A_N observed in *atquac1* plants (Table I), higher levels of sugars were also observed, which were properly remobilized during the dark period supporting higher R_d (Table I) and, in turn, leading to the enhanced growth observed in those plants (Fig. 1). However, it is important to mention that caution should be taken when analyzing such results obtained under well-controlled under situations. This is particularly true given that the growth benefit observed here (Fig. 1A), which was obtained under well-watered conditions, is not maintained under drought situations (Fig. 2C) most likely associated with a higher g_s and g_m observed in *atquac1* mutant plants. In contrast to the situations observed here, reductions in another stomatal channel protein (SLAC1) in rice were associated with increments in both A_N and g_s without any growth benefit under well-watered conditions (Kusumi et al., 2012) but culminated in lower productivity and yield of rice plants under field conditions. Taken together, these data indicate that an increased sensitivity to water limitations episodes associated with higher g_s and g_m can exceed the enhanced CO_2 assimilation under less favorably environments. Accordingly, our understanding of plant responses to water limitation is still fragmentary, most likely due to the complex responses involving adaptive changes and /or deleterious effects. Under field conditions, the responses can be synergistically or antagonistically modified by the interaction with other plants and/or superimposition of other stresses and therefore caution should be taken when interpreting the results described here and as such further investigation should be performed within the context of understanding the stomata responses to water stress.

Regarding to the nitrogen metabolism, it has been demonstrated an inverse relationship between amino acid contents and growth, given that even under nitrogen starvation (which leads to reduced growth), the amino acid levels have been shown to increase without changes in Rubisco activation, total protein, and chlorophyll contents (Tschoep et al., 2009). Interestingly, increases

in both A_N and growth in *atquac1* plants were neither followed by changes in chlorophyll, amino acid, or total soluble protein content (Supplemental Figs. S4 and S5), nor by changes in Rubisco activation state (Table III), highlighting that the increases in A_N were indeed associated with lower diffusional limitations (Table II). Furthermore, similar values of J_{max}:V_{cmax} ratio (Table II) and unchanging activities of some enzymes related to photosynthetic metabolism (e.g. Rubisco) are consistent with a photosynthetic functional balance since plants are able to adjust Rubisco content/activation and other photosynthetic machinery components to maintain the balance among the enzymatic reactions (e.g. Rubisco) and light harvesting (e.g. chlorophylls; Stitt and Schulze, 1994). Collectively, our results suggest that inefficient regulation of the stomatal closure via repression of *AtQUAC1* culminates in higher growth and photosynthetic rates through increased g_m and g_s, albeit promoting minor changes on carbon metabolism. This hypothesis is illustrated in Figure 7 and would hence explain why the accumulation of organic acids, in special malate within the guard cells, will culminate with a longer stomatal aperture in *atquac1* plants. This model further suggests that increased A_N is likely related to the maintenance of a high chloroplastic CO_2 concentration, ultimately leading to growth enhancement. It should be borne in mind that the changes observed in several sugars, as well as in dark respiration in *atquac1* plants can, at least partially, explain the higher growth rates. The exact mechanism by which changes in organic acid transport induced simultaneous changes in both g_s and g_m remains as yet unclear; however, it seems reasonable to anticipate this might be related to an as-yet-unknown signaling compound associated with higher photosynthetic rates.

MATERIALS AND METHODS

Plant Material and Growth Conditions

All Arabidopsis (*Arabidopsis thaliana*) plants used here were of the Colombia ecotype (Col-0) background. Seeds were surface-sterilized and imbibed for 2 d at 4°C in the dark on agar plates containing half-strength Murashige and Skoog media (Murashige and Skoog, 1962). Seeds were subsequently germinated and grown in a growth chamber under short-day conditions (8 h/16 h of light/dark) with 150 μmol m^{-2} s^{-1} white light, 22°C/20°C throughout the day/night cycle, and 60% relative humidity. The T-DNA mutant lines *atquac1-1* (SM_3_38592) and *atquac1-2* (SM_3_1713) were obtained from the John Innes Centre JIC collection (Tissier et al., 1999) and were previously described (Meyer et al., 2010). Plants with reduced expression of *AtQUAC1* were compared with plants that genotyped as wild-type (WT-like) during homozygous screening by PCR (for details, see Meyer et al., 2010). In all analyses performed, *atquac1-1* and *atquac1-2* mutant lines were directly compared with the corresponding WT lines (WT-like-1 and WT-like-2, respectively). The abundance of transcripts was confirmed by semiquantitative PCR using specific primers pairs designed to span the T-DNA insertion site of the two mutant loci (for details, see Supplemental Fig. S1).

Growth Analysis

Whole rosettes from 5-week-old plants were harvested and the RDW, LA, SLA, RGR were evaluated. LA was measured by digital image method using a scanner (Hewlett-Packard Scanjet G2410) and the images were after processed using the Rosette Tracker software (De Vylder et al., 2012). SLA and RGR, which is the net dry weight increase per unit dry weight per day (g g^{-1} day^{-1}), were calculated using the classical approach described by Hunt et al. (2002) with the following equations:

$$\mathrm{SLA}\left(\mathrm{m^2\ kg^{-1}}\right) = \frac{\mathrm{LA}}{\mathrm{LDW}^*}$$

*LDW = Leaves dry weight

$$\mathrm{RGR}\left(\mathrm{g\ g^{-1}\ day^{-1}}\right) = \frac{ln\mathrm{RDW}_2 - ln\mathrm{RDW}_1}{t_2 - t_1}$$

RDW_1 was measured 20 d after germination when the rosettes are expected to be with 20% of its final size (Boyes et al., 2001).

Stomatal Density and Stomatal Index

After 2 h of illumination in the night-day cycle described above, leaf impressions were taken from the abaxial surface of the ninth leaf totally expanded with dental resin imprints (Berger and Altmann, 2000). Nail polish copies were made using a colorless glaze (Von Groll et al., 2002), and the images were taken with a digital camera (Axiocam MRc) attached to a microscope (Zeiss, model AX10). The measurements were performed on the images using the Cell^P software (Soft Imaging System). Stomatal density and stomatal index (the ratio of stomata to stomata plus other epidermal cells) were determined in at least 10 fields of 0.04 mm^2 per leaf from eight different plants.

Gas Exchange and Chlorophyll Fluorescence Measurements

Gas exchange parameters were determined simultaneously with chlorophyll *a* fluorescence measurements using an open-flow infrared gas exchange analyzer system (LI-6400XT; LI-COR) equipped with an integrated fluorescence chamber (LI-6400-40; LI-COR). Instantaneous gas exchanges were measured after 1 h illumination during the light period under 700 μmol m^{-2} s^{-1} at the leaf level (light saturation) of PPFD, determined by *A*/PPFD curves (net photosynthesis (A_N) in response to PPFD curves; Supplemental Fig. S3; Supplemental Table S1). The reference CO_2 concentration was set at 400 μmol CO_2 mol^{-1} air. All measurements were performed using the 2 cm^2 leaf chamber at 25°C, and the leaf-to-air vapor pressure deficit was kept at 1.2 to 2.0 kPa, while the amount of blue light was set to 10% PPFD to optimize stomatal aperture.

The initial fluorescence (F_0) was measured by illuminating dark-adapted leaves (1 h) with weak modulated measuring beams (0.03 μmol m^{-2} s^{-1}). A saturating white light pulse (8000 μmol m^{-2} s^{-1}) was applied for 0.8 s to obtain the maximum fluorescence (F_m), from which the variable-to-maximum chlorophyll fluorescence ratio was then calculated: $F_v/F_m=[(F_m - F_0)/F_m)]$. In light-adapted leaves, the steady-state fluorescence yield (F_s) was measured with the application of a saturating white light pulse (8000 μmol m^{-2} s^{-1}) to achieve the light-adapted maximum fluorescence (F_m'). A far-red illumination (2 μmol m^{-2} s^{-1}) was applied after turn off the actinic light to measure the light-adapted initial fluorescence (F_0'). The capture efficiency of excitation energy by open PSII reaction centers (F_v'/F_m') was estimated following Logan et al. (2007) and the actual PSII photochemical efficiency (ϕ_{PSII}) was estimated as $\phi_{PSII} = (F_m' - F_s)/F_m'$ (Genty et al., 1989).

As the ϕ_{PSII} represents the number of electrons transferred per photon absorbed in the PSII, the electron transport rate (J_{flu}) was calculated as $J_{flu} = \phi_{PSII} \cdot \alpha \cdot \beta \cdot PPFD$, where α is leaf absorptance and β reflects the partitioning of absorbed quanta between PSII and PSI, and the product $\alpha\beta$ was adopted as described in the literature for Arabidopsis as equal to 0.451 (Flexas et al., 2007).

Dark respiration (R_d) was measured using the same gas exchange system as described above after at least 1 h during the dark period and it was divided by two ($R_d/2$) to estimate the mitochondrial respiration rate in the light (R_L; Niinemets et al., 2005, 2006; Niinemets et al., 2009).

A/PPFD curves were initiated at ambient CO_2 concentration (C_a) of 400 μmol mol^{-1} and PPFD of 600 μmol m^{-2} s^{-1}. Then, the PPFD was increased to 1000 μmol m^{-2} s^{-1} and after decreased until 0 μmol m^{-2} s^{-1} (11 different PPFD steps). Simultaneously chlorophyll *a* fluorescence parameters were obtained (Yin et al., 2009). The responses of A_N to C_i (A/C_i curves) were performed at 700 μmol m^{-2} s^{-1} at 25°C under ambient O_2. Briefly, the measurements started at ambient CO_2 concentration (C_a) of 400 μmol mol^{-1} and once the steady state was reached, C_a was decreased stepwise to 50 μmol mol^{-1}. Upon completion of the measurements at low C_a, C_a was returned to 400 μmol mol^{-1} to restore the

original A_N. Next, C_a was increased stepwise to1600 μmol mol^{-1} in a total of 13 different C_a values (Long and Bernacchi, 2003). Corrections for the leakage of CO_2 into and water vapor out of the leaf chamber of the LI-6400 were applied to all gas exchange data as described by Rodeghiero et al. (2007). A/C_i and A_N/PPFD curves were obtained using the ninth leaf totally expanded from ten different plants per genotype in two independent assays (five plants in each assay).

Estimation of Mesophyll Conductance (g_m), Maximum Rate of Carboxylation (V_{cmax}), Maximum Rate of Carboxylation Limited by Electron Transport (J_{max}), and Photosynthetic Limitations

The concentration of CO_2 in the carboxylation sites (C_c) was calculated following Harley et al. (1992) as:

$$C_c = \left(\Gamma^*\left(J_{flu} + 8(A_N + R_L)\right)\right) \Big/ \left(J_{flu} - 4(A_N + R_L)\right)$$

where the conservative value of Γ^* for Arabidopsis was taken from Walker et al. (2013). Then, g_m was estimated as the slope of the A_N versus $C_i - C_c$ relationship as:

$$g_m = A_N/(C_i - C_c)$$

Thus, estimated g_m is an averaged value over the points used in the relationship ($C_i < 300$ μmol mol^{-1}).

Given that current methods for estimating g_m include several assumptions as well as technical limitations and sources of error that need to be considered to obtain reliable values (Pons et al., 2009), g_m was estimated by the Ethier and Livingston (2004) method, which fits A_N/C_i curves with a nonrectangular hyperbola version Farquhar-von Caemmerer-Berry FvCB model, based on the hypothesis that g_m reduces the curvature of the Rubisco-limited portion of an A_N/C_i curve.

From A_N/C_i and A_N/C_c curves, the maximum carboxylation velocity (V_{cmax}) and the maximum capacity for electron transport rate (J_{max}) were calculated by fitting the mechanistic model of CO_2 assimilation (Farquhar et al., 1980) using the C_i or C_c-based temperature dependence of kinetic parameters of Rubisco (K_c and K_o; Walker et al., 2013). Then V_{cmax}, J_{max}, and g_m were normalized to 25°C using the temperature response equations from (Sharkey et al., 2007).

The photosynthetic limitations estimated based on the approach described by Grassi and Magnani (2005). This method uses the values of A_N, g_s, g_m, V_{cmax}, Γ^*, C_c, and $K_m = K_c\ (1 + O/K_o)$ and permits the partitioning into the functional components of photosynthetic constraints related to stomatal (l_s), mesophyll (l_m), and biochemical (l_b) limitations:

$$l_s = \frac{\left(\frac{g_{tot}}{g_s} \times \frac{\partial A_N}{\partial C_c}\right)}{\left(g_{tot} + \frac{\partial A_N}{\partial C_c}\right)}$$

$$l_m = \frac{\left(\frac{g_{tot}}{g_m} \times \frac{\partial A_N}{\partial C_c}\right)}{\left(g_{tot} + \frac{\partial A_N}{\partial C_c}\right)}$$

$$l_b = \frac{g_{tot}}{\left(g_{tot} + \frac{\partial A_N}{\partial C_c}\right)}$$

g_{tot} is the total conductance to CO_2 from ambient air to chloroplasts (g_{tot}=1/[(1/g_s) + (1/g_m)]). The fraction $\partial A_N/\partial C_c$ was calculated as:

$$\frac{\partial A_N}{\partial C_c} = \frac{\left[V_{cmax}(\Gamma^* + K_m)\right]}{(C_c + K_m)}$$

Stomatal Opening and Closing Kinetics Measurements

The g_s values were recorded at intervals of 1 min using the same gas-exchange system described above. The g_s responses to dark/light/dark transitions were measured in plants adapted to dark, at least for 2 h. The light in the chamber was kept turned off, and then turned on and then off for 10/60/60 min. The CO_2 concentration in the chamber was 400 μmol mol^{-1} air. For responses to CO_2 concentration, transitions leaves were exposed to 400/800/400 μmol CO_2 mol^{-1} air for 10/60/40 min under PPFD of 150 μmol m^{-2} s^{-1}.

Water Loss Measurements

For water loss measurements, the weight of detached rosettes, incubated abaxial side up under the same growth conditions described above, were determined over 4 h at the indicated time points. Water loss was calculated as a percentage of the initial fresh weight (Araújo et al., 2011b).

Determination of Metabolite Levels

Whole rosettes were harvested in different times along of the light/dark cycle (0, 4, 8, 16, and 24 h). Rosettes were flash-frozen in liquid nitrogen and stored at −80°C until further analyses. Metabolite extraction was performed by rapid grinding in liquid nitrogen and immediate addition of the appropriate extraction buffer. The levels of starch, Suc, Fru, and Glc in the leaf tissues were determined exactly as described previously (Fernie et al., 2001). Malate and fumarate were determined exactly as detailed by Nunes-Nesi et al. (2007). Proteins and amino acids were determined as described previously (Gibon et al., 2004b). The levels of others metabolites were quantified by GC-MS as described by Roessner et al. (2001), whereas photosynthetic pigments were determined exactly as described before (Porra et al., 1989).

Analyses of Enzymatic Activities

The enzymatic extract was prepared as previously described (Gibon et al., 2004a). Rubisco, PGK, transketolase, NADP-GAPDH, NAD-MDH, NADP-MDH, and Susy activities were determined as described by Sulpice et al. (2007), Burrell et al. (1994), Gibon et al. (2004a), Leegood and Walker (1980), Jenner et al. (2001), Scheibe and Stitt (1988), and Zrenner et al. (1995), respectively.

Isolation of Guard-Cell-Enriched Epidermal Fragments

The isolation of guard-cell-enriched epidermal fragments was performed as described previously (Pandey et al., 2002) with minor adaptations. Fully expanded leaves from four rosettes per sample were blended for 1 min and then for 30 s to 1 min (twice for 30 s) using a warring blender (Phillips, RI 2044) with an internal filter to clarify the epidermal fragments of mesophyll and fibrous cells. Subsequently, epidermal fragments were collected on a nylon membrane (200 μm mesh) and washed to avoid apoplast contamination before being frozen in liquid nitrogen. This protocol resulted in a guard cell purity of approximately 98% as assessed by Antunes et al. (2012).

qRT-PCR

qRT-PCR analysis was performed with total RNA isolated from epidermal fragments using the TRizol reagent (Ambion, Life Technology) following the manufacturer's manual. The integrity of the RNA was checked on 1% (w/v) agarose gels, and the concentration was measured before and after DNase I digestion using a spectrophotometer. Digestion with DNase I (Amplication Grade DNase I, Invitrogen) was performed according to the manufacturer's instructions. Subsequently, total RNA was reverse-transcribed into cDNA using Universal RiboClone cDNA Synthesis System (Promega) according to the respective manufacturer's protocols. For analysis of gene expression, the Power SYBR Green PCR Master Mix was used with the MicroAmp Optical 96-well Reaction Plate (both from Applied Biosystems) and MicroAmp Optical Adhesive Film (Applied Biosystems). The obtained cycle number at threshold was adjusted, and the estimation of the amplification efficiency was calculated using the Real-Time PCR Miner tool (Zhao and Fernald, 2005). The relative expression levels were normalized using the constitutively expressed genes *F-BOX* and *TIP41-LIKE* (Czechowski et al., 2005) and calculated using the ΔΔCT method. The primers used for qRT-PCR were designed using the QuantPrime software (Arvidsson et al., 2008) or taken from those described by Laanemets et al. (2013). Detailed primer information is described in Supplemental Table S2. The following genes were analyzed: *ALUMINUM ACTIVATED MALATE TRANSPORTER6* and *-9*, *ALMT6* and *ALMT9*; *ARABIDOPSIS THALIANA ATP-BINDING CASSETTE B14*, *AtABCB14* (Lee et al., 2008); *SLAC1*; *H$^+$-ATPASE1* and *-5*, *AHA1* and *AHA5* (Ueno et al., 2005); *POTASSIUM CHANNEL IN ARABIDOPSIS THALIANA1*, *KAT1* (Nakamura et al., 1995) and *KAT2*

(Pilot et al., 2001); *K+ TRANSPORTER1* and *-2*, *AKT1* and *AKT2* (Cao et al., 1995); *ARABIDOPSIS THALIANA K+ RECTIFYING CHANNEL1*, *AtKC1* (Reintanz et al., 2002); the K^+ outflow channel *GATED OUTWARDLY-RECTIFYING K^+ CHANNEL*, *GORK* (Ache et al., 2000); and *TWO-PORE CHANNEL1*, *TPC1* (Peiter et al., 2005).

Experimental Design and Statistical Analysis

The data were obtained from the experiments using a completely randomized design using all four genotypes (two WT-like genotypes × two T-DNA mutant lines *atquac1*). Data are expressed as the mean ± SE. Data were submitted to ANOVA and tested for significant ($P < 0.05$) differences using Student's *t* tests. All the statistical analyses were performed using the algorithm embedded into Excel (Microsoft).

Supplemental Data

The following supplemental materials are available.

Supplemental Figure S1. *AtQUAC1* gene structure and semiquantitative RT-PCR.

Supplemental Figure S2. Stomatal aperture and closure kinetics in response to light and CO_2.

Supplemental Figure S3. Net photosynthesis curves in response to PPFD.

Supplemental Figure S4. Total chlorophyll content and chlorophyll *a*/*b* ratio.

Supplemental Figure S5. Nitrate, free amino acids, and soluble protein content.

Supplemental Figure S6. Organic acid content.

Supplemental Table S1. Photosynthetic parameters obtained from light-response curves.

Supplemental Table S2. Primers utilized for qRT-PCR.

Supplemental Table S3. Relative metabolite levels determined by GC-MS.

Received July 7, 2015; accepted November 5, 2015; published November 5, 2015.

LITERATURE CITED

Ache P, Becker D, Ivashikina N, Dietrich P, Roelfsema MRG, Hedrich R (2000) GORK, a delayed outward rectifier expressed in guard cells of Arabidopsis thaliana, is a $K(^+)$-selective, $K(^+)$-sensing ion channel. FEBS Lett **486:** 93–98

Antunes WC, Provart NJ, Williams TCR, Loureiro ME (2012) Changes in stomatal function and water use efficiency in potato plants with altered sucrolytic activity. Plant Cell Environ **35:** 747–759

Araújo WL, Nunes-Nesi A, Fernie AR (2011a) Fumarate: multiple functions of a simple metabolite. Phytochemistry **72:** 838–843

Araújo WL, Nunes-Nesi A, Osorio S, Usadel B, Fuentes D, Nagy R, Balbo I, Lehmann M, Studart-Witkowski C, Tohge T, et al (2011b) Antisense inhibition of the iron-sulphur subunit of succinate dehydrogenase enhances photosynthesis and growth in tomato via an organic acid-mediated effect on stomatal aperture. Plant Cell **23:** 600–627

Arvidsson S, Kwasniewski M, Riaño-Pachón DM, Mueller-Roeber B (2008) QuantPrime–a flexible tool for reliable high-throughput primer design for quantitative PCR. BMC Bioinformatics **9:** 465

Berger D, Altmann T (2000) A subtilisin-like serine protease involved in the regulation of stomatal density and distribution in Arabidopsis thaliana. Genes Dev **14:** 1119–1131

Bergmann DC, Sack FD (2007) Stomatal development. Annu Rev Plant Biol **58:** 163–181

Bernacchi CJ, Portis AR, Nakano H, von Caemmerer S, Long SP (2002) Temperature response of mesophyll conductance. Implications for the determination of Rubisco enzyme kinetics and for limitations to photosynthesis in vivo. Plant Physiol **130:** 1992–1998

Blatt MR, Wang Y, Leonhardt N, Hills A (2014) Exploring emergent properties in cellular homeostasis using OnGuard to model K^+ and other ion transport in guard cells. J Plant Physiol **171:** 770–778

Borland AM, Hartwell J, Weston DJ, Schlauch KA, Tschaplinski TJ, Tuskan GA, Yang X, Cushman JC (2014) Engineering crassulacean acid metabolism to improve water-use efficiency. Trends Plant Sci **19:** 327–338

Bown HE, Watt MS, Mason EG, Clinton PW, Whitehead D (2009) The influence of nitrogen and phosphorus supply and genotype on mesophyll conductance limitations to photosynthesis in Pinus radiata. Tree Physiol **29:** 1143–1151

Boyes DC, Zayed AM, Ascenzi R, McCaskill AJ, Hoffman NE, Davis KR, Görlach J (2001) Growth stage-based phenotypic analysis of Arabidopsis: a model for high throughput functional genomics in plants. Plant Cell **13:** 1499–1510

Brandt B, Brodsky DE, Xue S, Negi J, Iba K, Kangasjärvi J, Ghassemian M, Stephan AB, Hu H, Schroeder JI (2012) Reconstitution of abscisic acid activation of SLAC1 anion channel by CPK6 and OST1 kinases and branched ABI1 PP2C phosphatase action. Proc Natl Acad Sci USA **109:** 10593–10598

Buckley TN, Warren CR (2014) The role of mesophyll conductance in the economics of nitrogen and water use in photosynthesis. Photosynth Res **119:** 77–88

Burrell M, Mooney P, Blundy M, Carter D, Wilson F, Green J, Blundy K, Rees T (1994) Genetic manipulation of 6-phosphofructokinase in potato tubers. Planta **194:** 95–101

Busch FA (2014) Opinion: the red-light response of stomatal movement is sensed by the redox state of the photosynthetic electron transport chain. Photosynth Res **119:** 131–140

Cao Y, Ward JM, Kelly WB, Ichida AM, Gaber RF, Anderson JA, Uozumi N, Schroeder JI, Crawford NM (1995) Multiple genes, tissue specificity, and expression-dependent modulation contribute to the functional diversity of potassium channels in Arabidopsis thaliana. Plant Physiol **109:** 1093–1106

Cowan IR, Troughton JH (1971) The relative role of stomata in transpiration and assimilation. Planta **97:** 325–336

Czechowski T, Stitt M, Altmann T, Udvardi MK, Scheible W-R (2005) Genome-wide identification and testing of superior reference genes for transcript normalization in Arabidopsis. Plant Physiol **139:** 5–17

De Vylder J, Vandenbussche F, Hu Y, Philips W, Van Der Straeten D (2012) Rosette tracker: an open source image analysis tool for automatic quantification of genotype effects. Plant Physiol **160:** 1149–1159

Du QS, Fan XW, Wang CH, Huang RB (2011) A possible CO_2 conducting and concentrating mechanism in plant stomata SLAC1 channel. PLoS One **6:** e24264

Duan B, Li Y, Zhang X, Korpelainen H, Li C (2009) Water deficit affects mesophyll limitation of leaves more strongly in sun than in shade in two contrasting Picea asperata populations. Tree Physiol **29:** 1551–1561

Ethier GJ, Livingston NJ (2004) On the need to incorporate sensitivity to CO^2 transfer conductance into the Farquhar–von Caemmerer–Berry leaf photosynthesis model. Plant Cell Environ **27:** 137–153

Farquhar GD, von Caemmerer S, Berry JA (1980) A biochemical model of photosynthetic CO_2 assimilation in leaves of C 3 species. Planta **149:** 78–90

Fernie AR, Martinoia E (2009) Malate. Jack of all trades or master of a few? Phytochemistry **70:** 828–832

Fernie AR, Roscher A, Ratcliffe RG, Kruger NJ (2001) Fructose 2,6-bisphosphate activates pyrophosphate: fructose-6-phosphate 1-phosphotransferase and increases triose phosphate to hexose phosphate cycling in heterotrophic cells. Planta **212:** 250–263

Flexas J, Barbour MM, Brendel O, Cabrera HM, Carriquí M, Díaz-Espejo A, Douthe C, Dreyer E, Ferrio JP, Gago J, et al (2012) Mesophyll diffusion conductance to CO_2: an unappreciated central player in photosynthesis. Plant Sci **193-194:** 70–84

Flexas J, Niinemets U, Gallé A, Barbour MM, Centritto M, Diaz-Espejo A, Douthe C, Galmés J, Ribas-Carbo M, Rodriguez PL, et al (2013) Diffusional conductances to CO_2 as a target for increasing photosynthesis and photosynthetic water-use efficiency. Photosynth Res **117:** 45–59

Flexas J, Ortuño MF, Ribas-Carbo M, Diaz-Espejo A, Flórez-Sarasa ID, Medrano H (2007) Mesophyll conductance to CO_2 in Arabidopsis thaliana. New Phytol **175:** 501–511

Flexas J, Ribas-Carbó M, Diaz-Espejo A, Galmés J, Medrano H (2008) Mesophyll conductance to CO_2: current knowledge and future prospects. Plant Cell Environ **31:** 602–621

Franks PJW, W Doheny-Adams T, Britton-Harper ZJ, Gray JE (2015) Increasing water-use efficiency directly through genetic manipulation of stomatal density. New Phytol **207:** 188–195

Galmés J, Conesa MÀ, Ochogavía JM, Perdomo JA, Francis DM, Ribas-Carbó M, Savé R, Flexas J, Medrano H, Cifre J (2011) Physiological and morphological adaptations in relation to water use efficiency in Mediterranean accessions of Solanum lycopersicum. Plant Cell Environ **34:** 245–260

Galmés J, Ochogavía JM, Gago J, Roldán EJ, Cifre J, Conesa MÀ (2013) Leaf responses to drought stress in Mediterranean accessions of Solanum lycopersicum: anatomical adaptations in relation to gas exchange parameters. Plant Cell Environ **36:** 920–935

Geiger D, Scherzer S, Mumm P, Marten I, Ache P, Matschi S, Liese A, Wellmann C, Al-Rasheid KAS, Grill E, et al (2010) Guard cell anion channel SLAC1 is regulated by CDPK protein kinases with distinct Ca^{2+} affinities. Proc Natl Acad Sci USA **107:** 8023–8028

Genty B, Briantais JM, Baker NR (1989) The relationship between the quantum yield of photosynthetic electron transport and quenching of chlorophyll fluorescence. Biochim Biophys Acta **990:** 87–92

Gibon Y, Blaesing OE, Hannemann J, Carillo P, Höhne M, Hendriks JH, Palacios N, Cross J, Selbig J, Stitt M (2004a) A Robot-based platform to measure multiple enzyme activities in Arabidopsis using a set of cycling assays: comparison of changes of enzyme activities and transcript levels during diurnal cycles and in prolonged darkness. Plant Cell **16:** 3304–3325

Gibon Y, Bläsing OE, Palacios-Rojas N, Pankovic D, Hendriks JH, Fisahn J, Höhne M, Günther M, Stitt M (2004b) Adjustment of diurnal starch turnover to short days: depletion of sugar during the night leads to a temporary inhibition of carbohydrate utilization, accumulation of sugars and post-translational activation of ADP-glucose pyrophosphorylase in the following light period. Plant J **39:** 847–862

Grassi G, Magnani F (2005) Stomatal, mesophyll conductance and biochemical limitations to photosynthesis as affected by drought and leaf ontogeny in ash and oak trees. Plant Cell Environ **28:** 834–849

Harley PC, Loreto F, Di Marco G, Sharkey TD (1992) Theoretical considerations when estimating the mesophyll conductance to CO_2 flux by analysis of the response of photosynthesis to CO_2. Plant Physiol **98:** 1429–1436

Hedrich R, Marten I (1993) Malate-induced feedback regulation of plasma membrane anion channels could provide a CO_2 sensor to guard cells. EMBO J **12:** 897–901

Hedrich R, Marten I, Lohse G, Dietrich P, Winter H, Lohaus G, Heldt HW (1994) Malate-sensitive anion channels enable guard-cells to sense changes in the ambient CO_2 concentration. Plant J **6:** 741–748

Hetherington AM (2001) Guard cell signaling. Cell **107:** 711–714

Hunt R, Causton DR, Shipley B, Askew AP (2002) A modern tool for classical plant growth analysis. Ann Bot (Lond) **90:** 485–488

Imes D, Mumm P, Böhm J, Al-Rasheid KAS, Marten I, Geiger D, Hedrich R (2013) Open stomata 1 (OST1) kinase controls R-type anion channel QUAC1 in Arabidopsis guard cells. Plant J **74:** 372–382

Jenner HL, Winning BM, Millar AH, Tomlinson KL, Leaver CJ, Hill SA (2001) NAD malic enzyme and the control of carbohydrate metabolism in potato tubers. Plant Physiol **126:** 1139–1149

Jin SH, Huang JQ, Li XQ, Zheng BS, Wu JS, Wang ZJ, Liu GH, Chen M (2011) Effects of potassium supply on limitations of photosynthesis by mesophyll diffusion conductance in Carya cathayensis. Tree Physiol **31:** 1142–1151

Kim T-H, Böhmer M, Hu H, Nishimura N, Schroeder JI (2010) Guard cell signal transduction network: advances in understanding abscisic acid, CO_2, and Ca^{2+} signaling. Annu Rev Plant Biol **61:** 561–591

Kollist H, Nuhkat M, Roelfsema MRG (2014) Closing gaps: linking elements that control stomatal movement. New Phytol **203:** 44–62

Kusumi K, Hirotsuka S, Kumamaru T, Iba K (2012) Increased leaf photosynthesis caused by elevated stomatal conductance in a rice mutant deficient in SLAC1, a guard cell anion channel protein. J Exp Bot **63:** 5635–5644

Laanemets K, Wang Y-F, Lindgren O, Wu J, Nishimura N, Lee S, Caddell D, Merilo E, Brosche M, Kilk K, et al (2013) Mutations in the SLAC1 anion channel slow stomatal opening and severely reduce K^+ uptake channel activity via enhanced cytosolic [Ca^{2+}] and increased Ca^{2+} sensitivity of K^+ uptake channels. New Phytol **197:** 88–98

Lawson T, Simkin AJ, Kelly G, Granot D (2014) Mesophyll photosynthesis and guard cell metabolism impacts on stomatal behaviour. New Phytol **203:** 1064–1081

Lee M, Choi Y, Burla B, Kim YY, Jeon B, Maeshima M, Yoo JY, Martinoia E, Lee Y (2008) The ABC transporter AtABCB14 is a malate importer and modulates stomatal response to CO_2. Nat Cell Biol **10:** 1217–1223

Leegood RC, Walker DA (1980) Autocatalysis and light activation of enzymes in relation to photosynthetic induction in wheat chloroplasts. Arch Biochem Biophys **200:** 575–582

Lisec J, Schauer N, Kopka J, Willmitzer L, Fernie AR (2006) Gas chromatography mass spectrometry-based metabolite profiling in plants. Nat Protoc **1:** 387–396

Logan BA, Adams WW, Demmig-Adams B (2007) Avoiding common pitfalls of chlorophyll fluorescence analysis under field conditions. Funct Plant Biol **34:** 853–859

Long SP, Bernacchi CJ (2003) Gas exchange measurements, what can they tell us about the underlying limitations to photosynthesis? Procedures and sources of error. J Exp Bot **54:** 2393–2401

Martinoia E, Meyer S, De Angeli A, Nagy R (2012) Vacuolar transporters in their physiological context. Annu Rev Plant Biol **63:** 183–213

Martins SCV, Galmés J, Molins A, DaMatta FM (2013) Improving the estimation of mesophyll conductance to CO_2: on the role of electron transport rate correction and respiration. J Exp Bot **64:** 1–14

Medeiros DB, Daloso DM, Fernie AR, Nikoloski Z, Araújo WL (2015) Utilizing systems biology to unravel stomatal function and the hierarchies underpinning its control. Plant Cell Environ **38:** 1457–1470

Meyer S, Mumm P, Imes D, Endler A, Weder B, Al-Rasheid KAS, Geiger D, Marten I, Martinoia E, Hedrich R (2010) AtALMT12 represents an R-type anion channel required for stomatal movement in Arabidopsis guard cells. Plant J **63:** 1054–1062

Mumm P, Imes D, Martinoia E, Al-Rasheid KAS, Geiger D, Marten I, Hedrich R (2013) C-terminus-mediated voltage gating of Arabidopsis guard cell anion channel QUAC1. Mol Plant **6:** 1550–1563

Murashige T, Skoog F (1962) A revised medium for a rapid growth and bioassays with tobacco tissues cultures. Physiol Plant **15:** 473–497

Nakamura RL, McKendree WL Jr, Hirsch RE, Sedbrook JC, Gaber RF, Sussman MR (1995) Expression of an Arabidopsis potassium channel gene in guard cells. Plant Physiol **109:** 371–374

Negi J, Matsuda O, Nagasawa T, Oba Y, Takahashi H, Kawai-Yamada M, Uchimiya H, Hashimoto M, Iba K (2008) CO_2 regulator SLAC1 and its homologues are essential for anion homeostasis in plant cells. Nature **452:** 483–486

Niinemets Ü, Cescatti A, Rodeghiero M, Tosens T (2005) Leaf internal diffusion conductance limits photosynthesis more strongly in older leaves of Mediterranean evergreen broad-leaved species. Plant Cell Environ **28:** 1552–1566

Niinemets U, Cescatti A, Rodeghiero M, Tosens T (2006) Complex adjustments of photosynthetic potentials and internal diffusion conductance to current and previous light availabilities and leaf age in Mediterranean evergreen species Quercus ilex. Plant Cell Environ **29:** 1159–1178

Niinemets U, Díaz-Espejo A, Flexas J, Galmés J, Warren CR (2009) Role of mesophyll diffusion conductance in constraining potential photosynthetic productivity in the field. J Exp Bot **60:** 2249–2270

Nunes-Nesi A, Carrari F, Gibon Y, Sulpice R, Lytovchenko A, Fisahn J, Graham J, Ratcliffe RG, Sweetlove LJ, Fernie AR (2007) Deficiency of mitochondrial fumarase activity in tomato plants impairs photosynthesis via an effect on stomatal function. Plant J **50:** 1093–1106

Pandey S, Wang X-Q, Coursol SA, Assmann SM (2002) Preparation and applications of Arabidopsis thaliana guard cell protoplasts. New Phytol **153:** 517–526

Pandey S, Zhang W, Assmann SM (2007) Roles of ion channels and transporters in guard cell signal transduction. FEBS Lett **581:** 2325–2336

Peguero-Pina JJ, Flexas J, Galmés J, Niinemets U, Sancho-Knapik D, Barredo G, Villarroya D, Gil-Pelegrín E (2012) Leaf anatomical properties in relation to differences in mesophyll conductance to $CO(_2)$ and photosynthesis in two related Mediterranean Abies species. Plant Cell Environ **35:** 2121–2129

Peiter E, Maathuis FJM, Mills LN, Knight H, Pelloux J, Hetherington AM, Sanders D (2005) The vacuolar Ca^{2+}-activated channel TPC1 regulates germination and stomatal movement. Nature **434:** 404–408

Penfield S, Clements S, Bailey KJ, Gilday AD, Leegood RC, Gray JE, Graham IA (2012) Expression and manipulation of phosphoenolpyruvate carboxykinase 1 identifies a role for malate metabolism in stomatal closure. Plant J **69:** 679–688

Pilot G, Lacombe B, Gaymard F, Cherel I, Boucherez J, Thibaud JB, Sentenac H (2001) Guard cell inward K^+ channel activity in arabidopsis involves expression of the twin channel subunits KAT1 and KAT2. J Biol Chem **276:** 3215–3221

Pons TL, Flexas J, von Caemmerer S, Evans JR, Genty B, Ribas-Carbó M, Brugnoli E (2009) Estimating mesophyll conductance to CO_2: methodology, potential errors and recommendations. J Exp Bot **60:** 2217–2234

Poorter H, Niinemets U, Poorter L, Wright IJ, Villar R (2009) Causes and consequences of variation in leaf mass per area (LMA): a meta-analysis. New Phytol **182:** 565–588

Porra RJ, Thompson WA, Kriedemann PE (1989) Determination of accurate extinction coefficients and simultaneous equations for assaying chlorophylls a and b extracted with four different solvents: verification

of the concentration of chlorophyll standards by atomic absorption spectroscopy. BBA - Bioenergetics **975:** 384–394

Raschke K (2003) Alternation of the slow with the quick anion conductance in whole guard cells effected by external malate. Planta **217:** 651–657

Reintanz B, Szyroki A, Ivashikina N, Ache P, Godde M, Becker D, Palme K, Hedrich R (2002) AtKC1, a silent Arabidopsis potassium channel α -subunit modulates root hair K^+ influx. Proc Natl Acad Sci USA **99:** 4079–4084

Rodeghiero M, Niinemets U, Cescatti A (2007) Major diffusion leaks of clamp-on leaf cuvettes still unaccounted: how erroneous are the estimates of Farquhar et al. model parameters? Plant Cell Environ **30:** 1006–1022

Roelfsema MRG, Hedrich R (2005) In the light of stomatal opening: new insights into 'the Watergate'. New Phytol **167:** 665–691

Roessner U, Luedemann A, Brust D, Fiehn O, Linke T, Willmitzer L, Fernie A (2001) Metabolic profiling allows comprehensive phenotyping of genetically or environmentally modified plant systems. Plant Cell **13:** 11–29

Sablowski R, Carnier Dornelas M (2014) Interplay between cell growth and cell cycle in plants. J Exp Bot **65:** 2703–2714

Sasaki T, Mori IC, Furuichi T, Munemasa S, Toyooka K, Matsuoka K, Murata Y, Yamamoto Y (2010) Closing plant stomata requires a homolog of an aluminum-activated malate transporter. Plant Cell Physiol **51:** 354–365

Scafaro AP, Von Caemmerer S, Evans JR, Atwell BJ (2011) Temperature response of mesophyll conductance in cultivated and wild Oryza species with contrasting mesophyll cell wall thickness. Plant Cell Environ **34:** 1999–2008

Scheibe R, Stitt M (1988) Comparison of NADP-malate dehydrogenase activation, QA reduction and O_2 evolution in spinach leaves. Plant Physiol Biochem **26:** 473–481

Schroeder JI, Delhaize E, Frommer WB, Guerinot ML, Harrison MJ, Herrera-Estrella L, Horie T, Kochian LV, Munns R, Nishizawa NK, et al (2013) Using membrane transporters to improve crops for sustainable food production. Nature **497:** 60–66

Sharkey TD, Bernacchi CJ, Farquhar GD, Singsaas EL (2007) Fitting photosynthetic carbon dioxide response curves for C(3) leaves. Plant Cell Environ **30:** 1035–1040

Stitt M, Schulze D (1994) Does Rubisco control the rate of photosynthesis and plant growth? An exercise in molecular ecophysiology. Plant Cell Environ **17:** 465–487

Sulpice R, Tschoep H, VON Korff M, Büssis D, Usadel B, Höhne M, Witucka-Wall H, Altmann T, Stitt M, Gibon Y (2007) Description and applications of a rapid and sensitive non-radioactive microplate-based assay for maximum and initial activity of D-ribulose-1,5-bisphosphate carboxylase/oxygenase. Plant Cell Environ **30:** 1163–1175

Thompson DS (2005) How do cell walls regulate plant growth? J Exp Bot **56:** 2275–2285

Tissier AF, Marillonnet S, Klimyuk V, Patel K, Torres MA, Murphy G, Jones JD (1999) Multiple independent defective suppressor-mutator transposon insertions in Arabidopsis: a tool for functional genomics. Plant Cell **11:** 1841–1852

Tschoep H, Gibon Y, Carillo P, Armengaud P, Szecowka M, Nunes-Nesi A, Fernie AR, Koehl K, Stitt M (2009) Adjustment of growth and central metabolism to a mild but sustained nitrogen-limitation in Arabidopsis. Plant Cell Environ **32:** 300–318

Ueno K, Kinoshita T, Inoue S, Emi T, Shimazaki K (2005) Biochemical characterization of plasma membrane H^+-ATPase activation in guard cell protoplasts of Arabidopsis thaliana in response to blue light. Plant Cell Physiol **46:** 955–963

Vahisalu T, Kollist H, Wang Y-F, Nishimura N, Chan W-Y, Valerio G, Lamminmäki A, Brosché M, Moldau H, Desikan R, et al (2008) SLAC1 is required for plant guard cell S-type anion channel function in stomatal signalling. Nature **452:** 487–491

Vahisalu T, Puzõrjova I, Brosché M, Valk E, Lepiku M, Moldau H, Pechter P, Wang Y-S, Lindgren O, Salojärvi J, et al (2010) Ozone-triggered rapid stomatal response involves the production of reactive oxygen species, and is controlled by SLAC1 and OST1. Plant J **62:** 442–453

Vavasseur A, Raghavendra AS (2005) Guard cell metabolism and CO_2 sensing. New Phytol **165:** 665–682

Vile D, Garnier E, Shipley B, Laurent G, Navas M-L, Roumet C, Lavorel S, Díaz S, Hodgson JG, Lloret F, et al (2005) Specific leaf area and dry matter content estimate thickness in laminar leaves. Ann Bot (Lond) **96:** 1129–1136

Villar R, Ruiz-Robleto J, Ubera JL, Poorter H (2013) Exploring variation in leaf mass per area (LMA) from leaf to cell: an anatomical analysis of 26 woody species. Am J Bot **100:** 1969–1980

Von Groll U, Berger D, Altmann T (2002) The subtilisin-like serine protease SDD1 mediates cell-to-cell signaling during Arabidopsis stomatal development. Plant Cell **14:** 1527–1539

Vrábl D, Vasková M, Hronková M, Flexas J, Šantrůček J (2009) Mesophyll conductance to $CO(_2)$ transport estimated by two independent methods: effect of variable $CO(_2)$ concentration and abscisic acid. J Exp Bot **60:** 2315–2323

Walker B, Ariza LS, Kaines S, Badger MR, Cousins AB (2013) Temperature response of in vivo Rubisco kinetics and mesophyll conductance in Arabidopsis thaliana: comparisons to Nicotiana tabacum. Plant Cell Environ **36:** 2108–2119

Warren CR (2008a) Soil water deficits decrease the internal conductance to CO_2 transfer but atmospheric water deficits do not. J Exp Bot **59:** 327–334

Warren CR (2008b) Stand aside stomata, another actor deserves centre stage: the forgotten role of the internal conductance to CO_2 transfer. J Exp Bot **59:** 1475–1487

Xiong TC, Hann CM, Chambers JP, Surget M, Ng CK-Y (2009) An inducible, modular system for spatio-temporal control of gene expression in stomatal guard cells. J Exp Bot **60:** 4129–4136

Yin X, Struik PC, Romero P, Harbinson J, Evers JB, VAN DER Putten PEL, Vos J (2009) Using combined measurements of gas exchange and chlorophyll fluorescence to estimate parameters of a biochemical C photosynthesis model: a critical appraisal and a new integrated approach applied to leaves in a wheat (Triticum aestivum) canopy. Plant Cell Environ **32:** 448–464

Zhao S, Fernald RD (2005) Comprehensive algorithm for quantitative real-time polymerase chain reaction. J Comput Biol **12:** 1047–1064

Zrenner R, Salanoubat M, Willmitzer L, Sonnewald U (1995) Evidence of the crucial role of sucrose synthase for sink strength using transgenic potato plants (Solanum tuberosum L.). Plant J **7:** 97–107